Available online at www.sciencedirect.com
SCIENCE DIRECT®
Journal of Nuclear Materials 341 (2005) 1–11
journal of nuclear materials
www.elsevier.com/locate/jnucmat

Structural properties and high-temperature reactions of the metastable Ω phase in Zr–Nb alloys

Gabriela Aurelio [a,*], Armando Fernández Guillermet [a], Gabriel J. Cuello [b], Javier Campo [c]

[a] Centro Atómico Bariloche and Consejo Nacional de Investigaciones Científicas y Técnicas, Av. Bustillo 9500, Bariloche (RN) 8400, Argentina
[b] Institut Laue Langevin, BP 156, F-38042 Grenoble, cedex 9, France
[c] Instituto de Ciencia de Materiales de Aragón, CSIC – Universidad de Zaragoza, 50009 Zaragoza, Spain

Received 15 October 2004; accepted 16 December 2004

Abstract

This article presents an experimental study and a systematic phenomenological analysis of the structural properties and the high-temperature reactions of the Ω phase formed by quenching ('q') bcc (β) Zr–Nb alloys. In the first part of the work an extensive database with lattice parameters (LPs) for the Ω^q and the untransformed β^q phase is developed on the basis of neutron diffraction measurements. Various striking features of the LP vs. composition relations are detected, and a new method of analysis is applied which involves the concept of a 'reference behavior' (RB) describing the probable properties of each individual phase if it were unaffected by the other structures in the heterogeneous alloys. In this way, a detailed evaluation is performed of the effects of Ω^q/β^q coherence strains upon the LPs of these two phases. In the second part of the work, neutron thermodiffraction studies are reported of the structural properties of the $\Omega^q + \beta^q$ two-phase alloys at 300 K $\leqslant T \leqslant$ 650 K. Extensive LP vs. time results are discussed. On this basis, the structural properties of the Ω^a phase formed isothermally upon aging ('a') are established, and compared with those of the Ω^q phase. In addition, new information is discussed on the evolution of the $\Omega^a + \beta^a$ system toward thermodynamic equilibrium. Moreover, it is shown how the present method of analysis may also be used to obtain indirect information of both theoretical and practical interest. In particular, considerable evidence is presented indicating that the Nb content of the Ω^a phase decreases upon aging whereas that of β^a increases. Finally, it is shown how these composition changes might be used to reconcile much of the long-standing conflicting reports concerning the structural properties of the Ω^q and Ω^a metastable phases.

PACS: 61.50.ks; 61.12.Ld; 61.66.Dk; 64.60.My

1. Introduction

The phase stability trends in the periodic table, particularly in the transition metals (TMs), have been a

* Corresponding author.
E-mail address: gaurelio@cab.cnea.gov.ar (G. Aurelio).

0022-3115/$ - see front matter © 2005 Elsevier B.V. All rights reserved.
doi:10.1016/j.jnucmat.2004.12.001

matter of continuous theoretical interest [1]. The early studies focused on the structural sequence hcp → bcc → hcp → fcc which is observed from left to right across the non-magnetic TMs. Later, there was a growing interest in studying the stability of progressively more complex phases [2], in particular, those which form in alloys through structural transitions of one of the key phases mentioned above. This is the case of the Ω phase, which is observed experimentally at high pressure in pure Zr, Ti and Hf. The Ω phase also forms by quenching alloys of these elements with other TMs. Some physical properties of the Ω phase are well documented, and a classical review of the diffusionless bcc → Ω transition may be found, e.g., in Refs. [3,4]. More recently, the interest in a detailed account of the structural properties and the relative stability of the Ω and bcc phases in the TM elements has been renewed. Three main routes have been explored. The first one comprises studies using first-principle calculations of the electronic structure [5–7], and the second relies upon experiments at ambient conditions and high pressures [8]. The third route, which has its roots on the physico-chemical thermodynamics of alloys and other condensed systems, aims at establishing a critical interplay between the results of the other two, the experimental trends at finite temperatures and reactions leading to thermodynamic equilibrium [9]. In the spirit of the latter alternative, we study in the present work the structural systematics and high-temperature reactions of the Ω phase in a key TM alloy system, viz., the Zr–Nb system.

The Zr–Nb system has traditionally been considered as the prototype of the binary Ω forming alloys on the 4d TM series. The phase diagram [10] presents a stable high-temperature bcc (β) phase which forms various metastable structures upon quenching ('q') to room temperature (T_R), viz., the martensitically formed hcp (α^q) phase, the so-called 'athermal' Ω phase (Ω^q) and the untransformed β^q phase [11]. In addition, under isothermal heat treatments ('aging') at an aging temperature, $T_A > T_R$, diffusion-controlled reactions occur in the quenched alloys. In particular, the Ω phase can be induced by aging the quenched β^q phase in alloys with an appropriate Nb content [12–14].

The present work is part of a long-term research project focusing on the structural properties and relative thermodynamic stability of these various metastable phases in as-quenched and aged conditions. One of the main targets of this research line is the understanding of the composition dependence of the lattice parameters (LPs) of the metastable structures. The extensive experimental information reviewed below (Section 2.2) indicates that a simple Vegard's law type of behavior is observed in the quenched β^q phase [15]. On the other hand, the LPs of the Ω^q phase suggest deviations from Vegard's law, which have motivated a series of recent studies of the bonding-structure relations [6,7,16]. The results and implications of such work form the relevant background and provide the motivations of the present article (Section 2.3).

The structural properties of the 'isothermal' β^a and Ω^a phases formed by aging have been poorly known from direct measurements. Some attempts have been made in the past to obtain indirect information on the composition of the Ω^a phase coexisting with β^a [17,18]. In particular, Grad et al. [18] used the a_β vs. at.% Nb relation at T_R to infer the composition of the aged β^a phase, and then combined this information with the relative mass fractions of Ω^a and β^a in the two-phase alloys to estimate the composition of Ω^a. Their results pointed to the existence of some striking differences in the available LPs vs. at.% Nb relations between the Ω^q and Ω^a phases. However, in order to establish accurately the possible differences in behavior, the structural properties of these two phases should be studied on the same alloys, e.g., by focusing on the high-temperature reactions by which the Ω^q phase transforms irreversibly into Ω^a. In this spirit, the main goal of the present article is to develop a consistent picture of the structural properties of the Ω^q and Ω^a phases, by combining the analysis of an extensive structural database for Ω^q with new in situ studies of the reactions which occur upon evolution of this phase toward thermodynamic equilibrium at high temperature.

The work proceeds as follows. In the first place, we perform a full analysis of recently reported neutron diffraction (ND) data [11,15] on the β^q and Ω^q LPs in quenched alloys. The structural properties are modeled using an idealized – or 'reference' – behavior for the LP vs. composition relation (Section 4.1). Next, an experimental study is reported of the evolution toward thermodynamic equilibrium of a β + Ω two-phase Zr–Nb alloy. The quenched samples are subjected to heating-aging-cooling treatments, and extensive in situ ND measurements of the LPs are performed as functions of temperature and time. Besides, the expressions proposed to model the LPs of the β^q and Ω^q phases at room temperature are generalized to include temperature effects (Sections 4.3 and 5). With such interpretation scheme a picture of the isothermal reactions occurring at high temperature is developed, which is further tested against the current database with structural information on Ω^a (Section 6). In this way, new estimated values are obtained for the composition of the Ω^a particles in several quenched–aged–quenched Zr–Nb alloys. The article ends with a discussion of the composition dependence of LPs in the Ω^q and Ω^a phases and by demonstrating a possible use of the present results in obtaining estimates of direct metallurgical interest.

2. Phases, structures and bond-length systematics

2.1. Crystallographic basis and structural relations

The β phase, corresponding to a bcc structure, can be alternatively described using an hexagonal unit cell, which is shown schematically in Fig. 1(a). The LPs of the hexagonal cell, a_{bcc} and c_{bcc}, are related to the traditional cubic LP a_β as follows:

$$a_{bcc} = \sqrt{2}a_\beta \quad \text{and} \quad c_{bcc} = \tfrac{\sqrt{3}}{2}a_\beta. \tag{1}$$

In this representation the bcc structure has three atoms per unit cell located at $(0,0,0)$, $(\frac{1}{3},\frac{2}{3},\frac{1}{3})$ and $(\frac{2}{3},\frac{1}{3},\frac{2}{3})$. The athermal $\beta \rightarrow \Omega$ transformation occurring on quenching Zr-rich Zr–Nb alloys involves a change in the position of the inner atoms of the hexagonal cell. The magnitude of this change depends upon the composition of the alloy [11]. In general, the two inner atoms in the Ω phase are located at the so-called 'B-type' sites $(\frac{1}{3},\frac{2}{3},\frac{1}{3}+z)$ and $(\frac{2}{3},\frac{1}{3},\frac{2}{3}-z)$, with $0 \leqslant z \leqslant \frac{1}{6}$. The value $z = 1/6$ corresponds to the ideal Ω phase, which has hexagonal symmetry and is described by space group *P6/mmm*, as is the case of pure Zr [19–21] and Zr-rich Zr–Nb alloys [22,11]. When $0 < z < \frac{1}{6}$ the symmetry is trigonal, described by the space group $P\bar{3}m1$, as in more concentrated alloys [22,11]. Finally, the value $z = 0$ corresponds to the hexagonal representation of the bcc structure ($Im\bar{3}m$), as shown in Fig. 1(a).

Changes in the LPs of the hexagonal cell may also occur during the athermal $\beta \rightarrow \Omega$ transformation. In Zr–Nb alloys, this transformation does not reach completion on quenching, i.e., there always remains some untransformed β^q phase coexisting with Ω^q [11]. These structures have been shown to present well-defined orientation relationships, viz., the $[0\,0\,0\,1]_\Omega$ hexagonal axis is parallel to the $[1\,1\,1]_\beta$ cubic direction, and the $[1\,1\,\bar{2}\,0]_\Omega$ hexagonal direction is parallel to the $[1\,\bar{1}\,0]_\beta$ cubic direction [23]. Finally, there is in general a misfit between the β and Ω lattices, which will be expressed in this article by means of the relative differences $\Delta a/a = (a_\Omega - a_{bcc})/a_{bcc}$ and $\Delta c/c = (c_\Omega - c_{bcc})/c_{bcc}$ (Section 5.1).

2.2. Systematics of interatomic distances and chemical bonding considerations

The shortest interatomic distance in the Ω phase, $d_{B–B}$ (Fig. 1(b)), is related to the LPs and the z parameter of the Ω phase by the following geometrical relation:

$$d_{B–B} = \sqrt{\frac{a_\Omega^2}{3} + \left(\frac{1}{3} - 2z\right)^2 c_\Omega^2}. \tag{2}$$

For the ideal (i.e., hexagonal) Ω phase, the second term in Eq. (2) vanishes, and $d_{B–B}$ depends only on the a_Ω value. Grad et al. [27] reported that in quenched as well as in quenched-and-aged Zr–Nb alloys $d_{B–B}$ remains almost identical to that of the Ω phase of Zr. Moreover, this $d_{B–B}$ value was shown to correlate almost exactly with the covalent single bond-length for Zr, $D(1)$, entering into Pauling's bond length–bond number relation [24], a regularity that had been observed already by Jamieson [25] in the Ω phase of Zr. In order to account for these regularities, Grad et al. proposed a model for the Ω phase in Zr–Nb alloys, according to which the B-type sites are preferentially occupied by Zr atoms and the B–B bonding between these sites shows a significant covalent contribution [27]. This effect has been referred to by us as bonding-induced atomic ordering (BIAO) [26].

More recently, additional information of various kinds has been presented which provide new insight on the bond-length systematics of the Ω phase. In the first place, electronic structure calculations [7] indicate that the chemical bonding of the Ω phase in the TM series

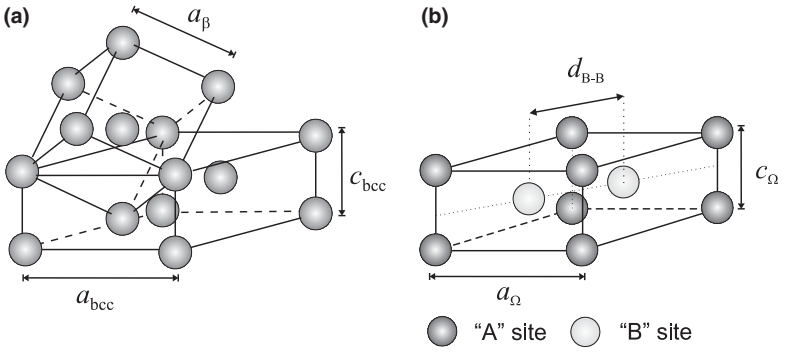

Fig. 1. (a) Geometrical relations between the hexagonal representation of the bcc structure and the traditional cubic cell. (b) The unit cell of the hexagonal Ω phase. The 'A'- and 'B'-type sites refer to the crystallographic sites 1a and 2d of the *P6/mmm* space group, respectively.

is significantly more complex than that hypothesized in the suggested model and in other approximate accounts of the Ω phase behavior [27]. Secondly, ND studies of the Ω phase in the isoelectronic Ti–V system [28,26] did not provide evidence of BIAO in the Ω phase. Thirdly, high resolution ND determinations of the composition dependence of the LPs in Zr–Nb alloys in an extended range of Nb contents indicate that d_{B-B} vs. Nb content relation deviates from the constancy suggested by Grad et al., reaching a minimum value which, in fact, is even smaller than $D(1)$ for Zr [22,11]. Moreover, a series of phenomenological studies [16] of the interatomic distances in the TMs showed that the correlation $d_{B-B} = D(1)$ might be understood by taking into account rather general properties of Pauling's bond length–bond number formalism as well as the relations between the Ω and β structures in these elements, without necessitating the hypothesis of a strongly covalent B–B bond.

2.3. Open problems and present methodology

From the recent experimental and theoretical studies reviewed above, a picture of the Ω phase has emerged [26,29] according to which the composition dependence of the structural properties does not differ significantly from what is observed in other metallic phases in TM alloys, which usually present a Vegard's law type of variation in the LPs. In this way, most of the experimental trends may be accounted for, but two main problems remain open, which provide the central motivation for the present study. Firstly, the LP vs. composition relations for the quenched Ω phase present small but striking deviations from linearity. This problem will be treated in Section 4, by performing a new type of analysis of the LP data for quenched alloys, and allowing for the possibility of coherence strains in the β + Ω two-phase systems. The second problem concerns the structural relations between the quenched and the aged Ω phase. This question will be dealt with by combining the additional insight gained on the quenched Ω phase (Section 4) with a new ND investigation of the reactions occurring upon aging. The experimental techniques and results are briefly described in the next section.

3. Experimental methods and results

3.1. Alloys, samples and heat-treatments

The measurements discussed in this article were performed on an alloy with a nominal Nb content of 10 at.% Nb (samples 1, 2 and 3). The alloy was prepared from Zr and Nb of 99.9% and 99.8% purity, respectively, in an arc furnace, on a water-cooled copper hearth, using non-consumable electrodes in a 350-Torr Ar atmosphere, and was remelted at least six times to favor homogeneity. Samples were cut into shavings of about 2 mm side length in order to approach the conditions of a powder-diffraction experiment. The shavings were wrapped up in Ta foils, doubly-encapsulated in quartz under high-purity Ar, annealed 1 h at 1273 K, and quenched in water by breaking the outer capsule.

The Nb content of the alloy was determined using a Cameca SX100 EPMA equipped with five wavelength-dispersive spectrometers at the Max-Planck Institut, Stuttgart. The content of O and N in the various samples was determined by a fusion method, using a LECO TC-36 analyzer. The results, listed in Table 1, indicate that the oxygen intake occurs during the sample preparation process and not during the subsequent heat treatments.

3.2. Neutron thermodiffractometry and data processing

The neutron thermodiffraction experiments were performed in the D1B two-axes diffractometer at the Institut Laue-Langevin, Grenoble, France. The neutron spectra were collected placing the ^{3}He multidetector of 400 cells in a cylindrical geometry centered at the sample. The angular span was of 80°, with steps of 0.2°. A Ge monochromator in the (3 1 1) reflection was used, obtaining a wavelength $\lambda \approx 1.28$ Å. This wavelength and the zero-shift were calibrated using a standard Al_2O_3 sample, which yielded $\lambda = 1.2899 \pm 0.0001$ Å. The samples were aged in a standard Vanadium furnace under vacuum of 1.8×10^{-4} mbar in order to prevent oxidation, which was verified after each aging treatment. The neutron flux on the sample was of about 10^6 n/(s cm^2), which allowed us to monitor the evolution dur-

Table 1
Chemical composition of the Zr–Nb alloy and the relevant temperatures in the present heat-treatments (Section 3.2)

Sample	Chemical composition					Reference temperatures (K)	
	at.% Nb	Before quenching		After quenching		T_A	T_{low}
		N [ppm]	O [ppm]	N [ppm]	O [ppm]		
1	10.4 ± 0.3	293	9800	404	8000	523	–
2						600	315
3						650	346

ing aging by diffraction patterns collected in 5 min. The samples were first kept for some minutes at $T = T_R$. After following different pathways, long aging treatments at $T = T_A$ were performed. Finally, the samples were air-cooled down to a temperature $T = T_{low}$. In Table 1 we list the corresponding T_A and T_{low} temperatures for each sample. The diffraction data, which amount to 42 diffractograms, were processed using the full-pattern analysis Rietveld method, with the program Fullprof [30]. The structural model which yielded the best refinements at high temperature consisted of a two-phase mixture of β phase ($Im\bar{3}m$) and Ω phase with hexagonal symmetry ($P6/mmm$). In both phases, the crystallographic sites were assigned an occupation related to the global composition of the alloy.

3.3. Experimental results

In the as-quenched state, the alloy studied experimentally in the present work consists of a two-phase mixture of $\beta^q + \Omega^q$, with a relative mass fraction of the Ω^q phase of about 80%, which makes it appropriate

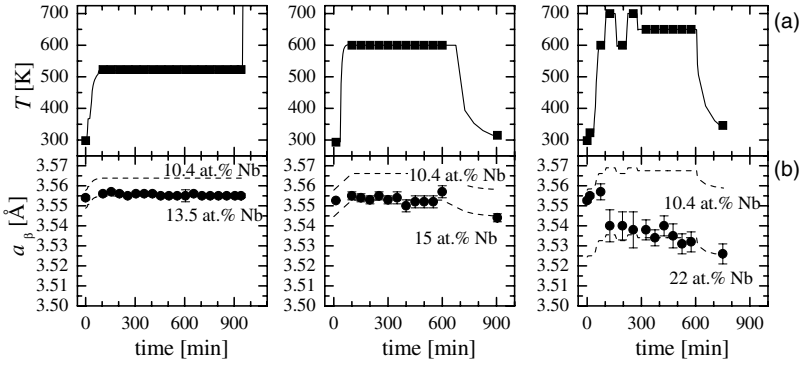

Fig. 2. (a) Heat-treatments applied to samples 1, 2 and 3 of an alloy with 10.4 at.% Nb. The solid lines represent the temperature of the samples, measured in 5-min time steps. Symbols represent series of 5-min neutron diffractograms at a given temperature, which were added up to enhance the statistics. (b) The experimental LP (symbols) of the β phase determined as function of time during the heat-treatments described in (a). The dashed lines represent the RB (Eq. (6)) for an alloy with the initial and the probable final compositions, as explained in Section 5.

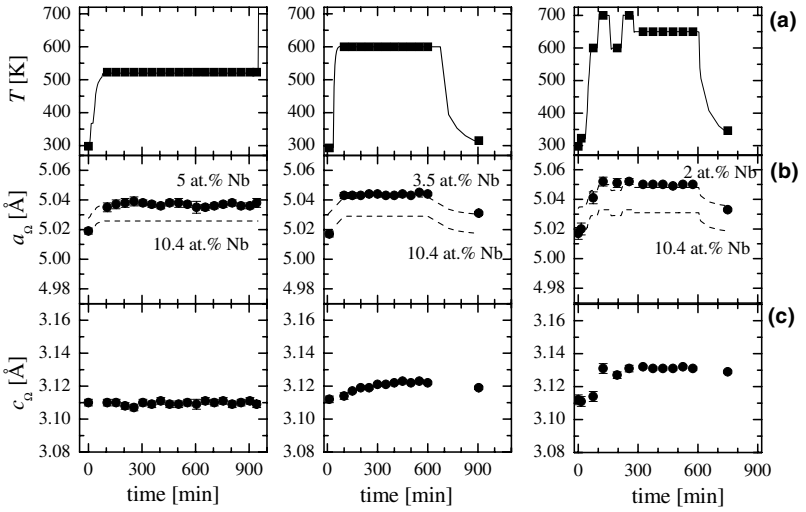

Fig. 3. (a) Heat-treatments applied to samples 1, 2 and 3 of an alloy with 10.4 at.% Nb. The solid lines represent the temperature of the samples, measured in 5-min time steps. Symbols represent series of 5-min neutron diffractograms at a given temperature, which were added up to enhance the statistics. (b,c) The experimental LPs a_Ω and c_Ω (symbols) of the Ω phase determined as a function of time during the heat-treatments described in (a). The dashed lines in (b) represent the RB (Eq. (7)) for an alloy with the initial and the probable final compositions, as explained in Section 5.

for investigating the evolution of this metastable phase during aging.

In Fig. 2(a) we present the temperature vs. time data corresponding to the heat-treatments applied to samples 1, 2 and 3. The solid lines represent the temperature of the samples, measured in 5-min time steps. The symbols represent series of 5-min neutron diffractograms at a given temperature which were added up to enhance the statistics. During the heat treatments, the constitution of the alloys remained a two-phase mixture of $\beta + \Omega$. In Fig. 2(b) we plot using symbols the LP a_β, and in Fig. 3(b) and (c) the LPs a_Ω and c_Ω, respectively, obtained in the Rietveld refinements. The dashed lines plotted in these figures will be discussed in Section 5.

4. Lattice parameter assessment and modeling

4.1. Individual phases in the quenched alloys at room temperature

In this section, a complete analysis is made of the LP database on quenched phases in Zr–Nb alloys obtained during the last years in our group [11,17,18,31,32], and by other authors [19,23,33–35]. The key purpose of the present and the next subsection is to develop a suitable reference for analyzing the data on each individual phase. In Figs. 4 and 5 we summarize the available LP vs. at.% Nb data for the athermal β and Ω phases induced by quenching to T_R, obtained from X-ray [23,33] and neutron [11,17,18,31,32] diffraction experiments.

The previous LP assessment of the Zr–Nb β^q phase performed by Grad et al. [36] by combining ND measurements in alloys with data on pure Zr and Nb, suggested that a_β follows a linear, Vegard's law-type of behavior as a function of the Nb content. The most recent a_β values reported by us [15] agree well with this behavior. We will refer to it as the 'reference behavior' (RB) for the β phase, represented in Fig. 4 using a solid line and described by the expression

$$a_\beta(x_{Nb}, T_R)\ [\text{Å}] = 3.5878(7) - 0.00288(3)x_{Nb}\ [\text{at.\%}]. \quad (3)$$

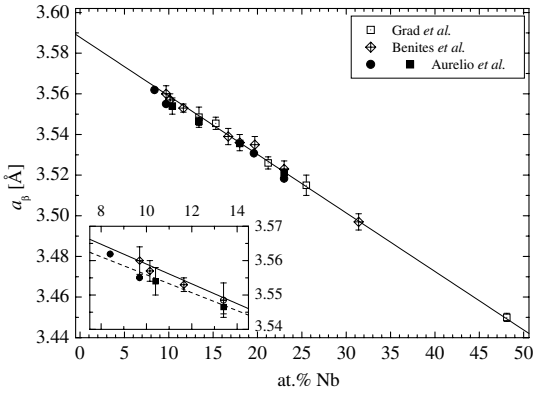

Fig. 4. Composition dependence of the LP a_β of the bcc (β^q) phase in Zr–Nb alloys quenched at T_R. The solid line represents the RB (Section 4.1) adopted for the β phase at room temperature, Eq. (3). The dashed line in the inset is only a guide to the eye (Section 4.2).

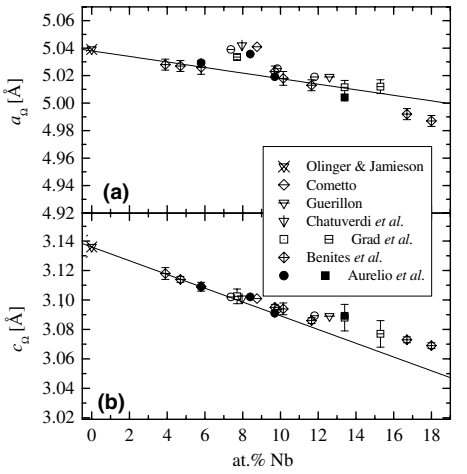

Fig. 5. Composition dependence of the LPs a_Ω (a) and c_Ω (b) of the Ω^q phase in quenched Zr–Nb alloys measured at T_R. The solid lines represent the RBs (Section 4.1) adopted for the Ω phase at room temperature, Eqs. (4) and (5).

In analogy, we will adopt for the quenched Ω phase a RB describing the probable LP variation with the Nb content. However, the possibility of coherence strains affecting the LP values should be considered. For that reason, we propose as a reference the variation of the LPs of an hypothetical Ω^q phase which is not subjected to significant Ω/β coherence strains. Information on such RB is provided by the LPs of the Ω phase of Zr and by the quenched alloys in the composition range $0 \leqslant x_{Nb} \leqslant 7$, where Ω^q occurs in the absence of β^q. In this range, Ω^q coexists with α^q, but no significant Ω^q/α^q coherence strains are believed to be present. A least-squares fitting procedure to the a_Ω value for pure Zr [19] as well as the available a_Ω measurements in binary alloys in the quoted composition range yields

$$a_\Omega(x_{Nb}, T_R)\ [\text{Å}] = 5.038(1) - 0.00202(2)x_{Nb}\ [\text{at.\%}] \quad (4)$$

and

$$c_\Omega(x_{Nb}, T_R)\ [\text{Å}] = 3.1360(1) - 0.00467(2)x_{Nb}\ [\text{at.\%}]. \quad (5)$$

In the remained of the present article, Eqs. (4) and (5) will be adopted to describe the RB for the Ω^q phase at room temperature.

4.2. Coherence strains in $\Omega^q + \beta^q$ quenched alloys

A detailed examination of our previous high resolution ND measurements of a_β (inset in Fig. 4) reveals a systematic deviation of the experimental values from the RB (Eq. (3)) in the range $8 < x_{Nb} < 14$. In addition, Fig. 5 shows that the a_Ω parameter of the Ω^q phase in $\beta^q + \Omega^q$ quenched alloys also deviates from a linear variation with Nb content in the range $7 < x_{Nb} < 11$. Looking for a possible connection between these features of the composition dependence of the LPs of the Ω^q and β^q coexisting phases, we compare in Fig. 6 the experimental a_Ω (filled symbols) and a_{bcc} values (open symbols) for at.% Nb < 14 measured in our group using ND. The a_{bcc} values were calculated by inserting the observed a_β (Fig. 4) into Eq. (1). The RBs adopted for each phase, described by Eqs. (3) and (4), are represented in Fig. 6 using solid lines. Fig. 6 shows that the deviations of the LPs a_Ω and a_{bcc} from their respective RB become particularly large in the range of coexistence of the Ω^q and β^q phases, viz., the a_Ω parameter increases considerably and a_{bcc} decreases, approaching each other. Moreover, the maximum deviations for the Ω phase are located at about 9 at.% Nb, i.e., in the composition range where the maximum amount of Ω^q phase is formed by quenching, viz., almost 80% [11]. Whereas the present analysis reveals strong β^q/Ω^q coherence strains in the $[1\,1\,0]_\beta$ direction, i.e., the direction of the a_Ω axis, the results in Fig. 5(b) indicate, however, that the c_Ω parameter is less affected by coherence strains in the $[1\,1\,1]_\beta$ direction.

Finally, we recall that for alloys with at.% Nb > 9 it is known to exist a symmetry change in the Ω phase [11,31], which could possibly explain the different slope shown by the LPs at higher Nb contents. This issue has been discussed in Ref. [11].

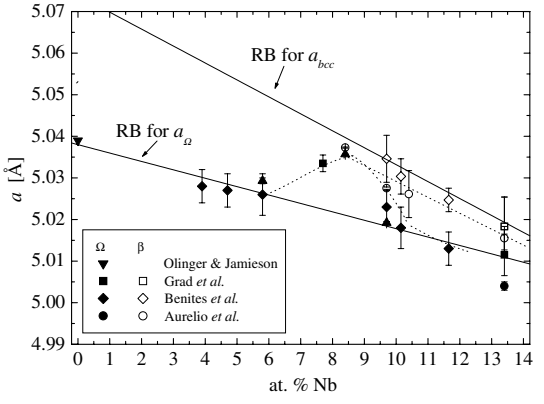

Fig. 6. Composition dependence of the LPs a_Ω (filled symbols) and a_{bcc} (open symbols), corresponding to the hexagonal representation of the β phase, in quenched Zr–Nb alloys. The upper and lower solid lines represent the RB for a_{bcc} and a_Ω, respectively, in quenched Zr–Nb alloys at T_R. The dashed lines are only guides to the eye.

4.3. Individual phases in aged alloys at high temperature

In order to analyze the evolution of the LPs of the β and Ω phases upon aging, thermal expansion effects have to be included in the RBs proposed in Section 4.1. Recently, a generalized form of Vegard's law was developed to treat the expansion of the β phase of single-phase quenched alloys [15]. With such an approach, it was possible to consistently account for the LP measurements on alloys quenched to T_R, in situ LP measurements on Zr–Nb alloys, and previously published thermal expansion data on the β phase of the elements Zr and Nb [15]. In accord with the results in Ref. [15] we will describe the temperature effects upon the RB for the β phase as follows:

$$a_\beta(x_{Nb}, T)\ [\text{Å}] = (3.5878(7) - 0.00288(3)x_{Nb}) \times \exp\left[6.8(5)\times 10^{-6}(T - T_R) + 1.0(2)\times 10^{-9}\left(T^2 - T_R^2\right)\right], \quad (6)$$

where T_R corresponds to room temperature, and the temperatures are in K.

Since a single-phase Ω alloy cannot be obtained by quenching at atmospheric pressure, a similar procedure cannot be applied to the Zr–Nb Ω phase. Therefore, an approximate method will be tested, in which temperature effects are estimated by assuming that in Zr-rich alloys, the LPs of the Ω phase vary with T as in the Ω phase of Zr. The properties of the latter are known after the work by Butz et al. [21], who determined the linear expansion coefficient along the a_Ω and the c_Ω-axes. By combining their results with Eqs. (4) and (5), the following expressions are obtained:

$$a_\Omega(x_{Nb}, T)\ [\text{Å}] = (5.038(1) - 0.00202(2)x_{Nb}) \times \exp[7.9(4)\times 10^{-6}(T - T_R)], \quad (7)$$

$$c_\Omega(x_{Nb}, T)\ [\text{Å}] = (3.1360(1) - 0.00467(2)x_{Nb}) \times \exp[3.5(3)\times 10^{-6}(T - T_R)]. \quad (8)$$

Eqs. (7) and (8) are considered a reasonably good approximation to the real properties of a Zr–Nb Ω phase which forms upon aging with a relatively low Nb content (see below). In the next subsection, Eqs. (6)–(8) will be used to analyze the experimental LPs of the Ω^a phase coexisting with β^a in the present alloy at high temperatures.

5. High-temperature reactions in Ω + β alloys

5.1. Evaluation of lattice parameters and coherence strains

In Fig. 2(b) we compare the LPs determined upon aging (symbols) with the predictions of Eq. (6) for the

β^a phase (dashed lines) in a Zr–Nb alloy with the initial composition, i.e., 10.4 at.% Nb and in an alloy with what we considered as the probable final composition. The latter was estimated as the value which inserted into Eq. (6) reproduces the a_β value measured at the final steps of the aging treatment. We note that the a_β values determined at T_A and those determined at T_{low} after air-cooling the aged samples fall almost exactly upon the same reference line, lending additional support to the description of thermal expansion effects in Zr–Nb β-phase alloys proposed in our previous work [15].

The comparison between experiments (symbols) and the predictions of Eq. (7) for the Ω^a phase (dashed lines) is given in Fig. 3(b). In this case, the probable final composition was estimated as the value which inserted into Eq. (7) reproduces the a_Ω value measured at the final steps of the aging treatment. Fig. 3 demonstrates that the LP difference between the values determined after the longest aging treatments and the measured after air-cooling to T_{low} are, in general, well accounted for by the calculated lines. This indicates that Eq. (7) provides a reasonably good first approximation to the true thermal expansion of a_Ω in this alloy.

In Fig. 7 we present the ratios $\Delta a/a$ and $\Delta c/c$ defined in Section 2, determined in samples 1, 2 and 3 upon aging at 523 K, 600 K and 650 K, respectively, as functions of aging time. Fig. 7 shows that in the as-quenched state the a_Ω parameter allows a high degree of coherence between the Ω particles and the β matrix, as discussed in Section 4.1. The c_Ω parameter, on the other hand, presents a larger misfit. Upon aging, both $(\Delta a/a)$ and $(\Delta c/c)$ increase, indicating a general lost of coherence between Ω^a and β^a, and the misfit increases with the aging temperature. In particular, Fig. 7 suggests that the coherence strains in the a_Ω direction are released during the early steps of the heat treatments.

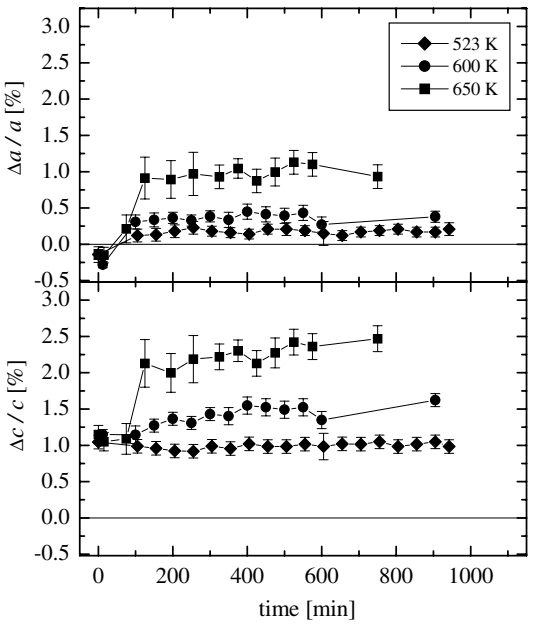

Fig. 7. The ratios $\Delta a/a = (a_\Omega - a_{bcc})/a_\Omega$ and $\Delta c/c = (c_\Omega - c_{bcc})/c_\Omega$ in samples 1, 2 and 3 of an alloy with 10.4 at.% Nb upon aging at 523 K, 600 K, and 650 K, respectively, as functions of aging time.

In summary, the high temperature ND data obtained in the present work (Figs. 2 and 3) indicate that significant changes in the LPs of the Ω and β phases occur upon the early steps of the high temperature agings. After relatively short aging times, the LPs reach stationary values. In the next subsection we use the present correlations to connect such LP behavior with composition changes expected to occur in the $\Omega^a + \beta^a$ alloys.

5.2. Diffusion reactions upon aging

It has long been believed that the β^a phase undergoes upon aging diffusion-controlled reactions, which increase its Nb content [12]. The key idea of the present work is that the reactions in β^a might be monitored through LP measurements, and by comparing those with suitable reference lines. The results in Fig. 2 indicate that as the aging temperature increases, a_β deviates progressively from the line corresponding to the initial composition, and the LP values fall on a line of higher Nb content, supporting the picture of a significant Nb enrichment in β^a during the aging process. Since the aged alloys consist of a two-phase mixture of $\beta^a + \Omega^a$, it is natural to search for evidence that the Ω phase concomitantly decreases its Nb content. Direct measurements of such depletion have not yet been available, but Fig. 3 shows that as the aging temperature increases, the a_Ω values shift toward reference lines consistent with a significant Nb depletion of the Ω^a phase. This observation is also supported by the recent results of a direct determination of the composition of aged Ω particles, performed using analytical transmission electron microscopy (TEM) [37]. In that work, an alloy with 9.6 at.% Nb quenched from 1273 K, aged at 773 K and quenched again to T_R was studied. X-ray microanalysis was used to measure the relative concentration of Nb in the Ω particles. We found [37] that as the aging time increases the mean Nb content in the Ω particles decreases significantly, which is in qualitative agreement with the present picture of a Nb transfer upon aging between the Ω^a and β^a phases.

In summary, the present results indicate that the Nb content of β^a (Ω^q) is larger than that of β^q (Ω^a). Qualitatively, these changes might be understood in thermodynamic terms by considering the schematic Gibbs energy vs. composition diagrams for these alloys [12]. In particular, a Zr-rich Ω phase is expected to be the stable phase in the absence of the α phase, as happens in Zr

[10]. In such case, the common tangent construction indicates that the alloy will be composed of a mixture of a metastable Zr-rich Ω phase and a Nb-rich β phase. Eventually, however, Ω^a will disappear in favor of the stable α phase. On the basis of the present as well as previous studies, including those in which the α^a phase was detected to form upon aging [15,40], a picture of the processes occurring upon aging $\beta^q + \Omega^q$ alloys may be developed, which is summarized by the following general reaction involving metastable phases,

$$\beta^q + \Omega^q \xrightarrow{\text{short aging times}} \beta^a + \Omega^a \xrightarrow{\text{long aging times}} \alpha^a + \beta^a. \qquad (9)$$

Finally, new TEM experiments are in progress which will be used in a quantitative test of the predictions of the RBs developed here [38], and of the suggested reaction scheme (Eq. (9)).

6. Concluding discussion of lattice parameter correlations for Ω phases

In the previous section we analyzed the LP data from the present in situ high-temperature aging experiments in terms of Eqs. (7) and (8). However, most of the previously reported LP studies of the aged Ω phase have been performed after quenching–aging–quenching to T_R experiments. In order to make contact with the extensive database developed in that type of studies, we apply a three-step procedure, as follows.

Firstly, by using the thermal expansion description adopted for the Ω phase (Section 4.3), we expressed the c_Ω values from the final steps of the aging treatments (Fig. 3) as c_Ω values at T_R. These room temperature values are plotted in Fig. 8 as functions of the Nb contents in Ω^a estimated from the a_Ω parameter (Section 5.1), and are compared with Eq. (5) (upper solid line) and with measured values on quenched alloys (open symbols). Fig. 8 shows that the c_Ω values for aged alloys agree within the experimental error with the reference line

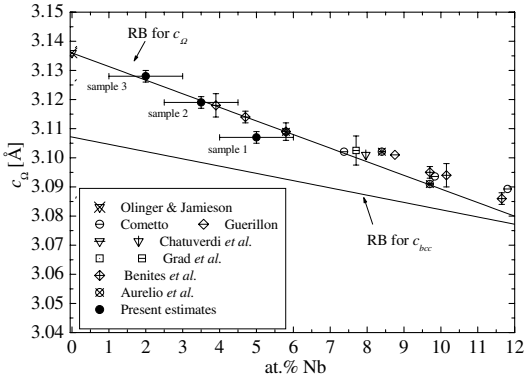

Fig. 8. Composition dependence of the lattice parameter c_Ω in quenched (open symbols) and aged (filled symbols) Zr–Nb alloys at T_R. The Nb content in the Ω^a phase was determined using the estimation procedure described in Section 5. The solid lines represent the RB for the c_Ω and c_{bcc} parameters.

for quenched alloys once the composition changes occurring upon aging have been accounted for. In particular, such a regular behavior holds for some datapoints in the composition range ($0 \leqslant x_{Nb} \leqslant 4$) in which the Ω^q phase cannot be obtained by quenching because of the formation of the competing martensitic α^q phase.

Secondly, we turn to the current LP database for Ω after quenched–aged–quenched to T_R experiments [12,13,17,18,39,40], which is summarized in Table 2. The Nb content of the Ω^a phase in those experiments was not determined, but may be inferred by inserting the reported a_Ω and c_Ω values into Eqs. (4) and (5). This method provides two probable Nb contents (x^Ω_{Nb}), which are in reasonably good agreement (Table 2), and indicate that the Nb concentration in Ω^a decreases upon aging down to a probable content falling in the range $0 \leqslant x^\Omega_{Nb} \leqslant 7$.

Thirdly, in order to further check the consistency of the predictive scheme developed, we consider the c_Ω/a_Ω

Table 2
Room temperature lattice parameters of the Ω phase determined after quenching–aging–quenching experiments by X-ray [12,13,39] and neutron diffraction [17,18,40] studies

Ref.	x^{alloy}_{Nb} [at.% Nb]	Aging conditions		LPs [Å]		Estimated x^Ω_{Nb} [at.% Nb]	
		T_A [K]	Time [h]	a_Ω	c_Ω	From a_Ω (Eq. (4))	From c_Ω (Eq. (5))
[33]	11.9	623	10	5.029	3.118	4.5	4
	17.3	673	0.8	5.039	3.127	0	2
[12]	7.5	673	40	5.036	3.127	1	2
	11.9	673	40	5.038	3.128	0	1.5
	17.3	673	40	5.033	3.129	2.5	1.5
[39]	14.8	648	168	5.036	3.130	1	1
[13]	29.6	673	300	5.030	3.120	4	3.5
[17]	9.7	673	39	5.038	3.134	0	0.5
[40]	9.7	773	0.7	5.036	3.130	1	1

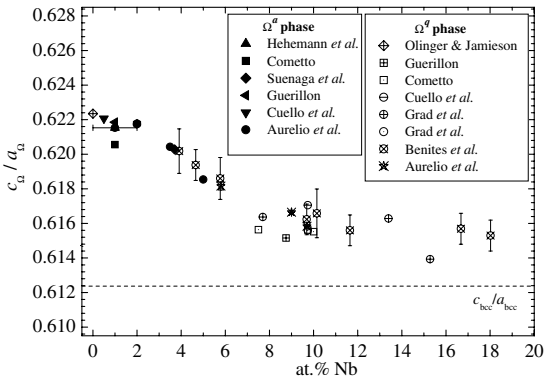

Fig. 9. Composition dependence of the c_Ω/a_Ω ratio in quenched (open symbols) and aged (filled symbols) Zr–Nb alloys at T_R. The Nb content in the Ω^a phase was determined using the estimation procedure described in Section 5. The horizontal dashed line represents the ratio c_{bcc}/a_{bcc} corresponding to the hexagonal representation of the cubic β phase, i.e., $c_\Omega/a_\Omega = \sqrt{3/8} = 0.6124$.

ratio for the Ω phase, and compare in Fig. 9 the values for aged alloys (filled symbols) with those for quenched alloys (open symbols). In this figure, the c_Ω/a_Ω ratio for aged alloys has been plotted as function of the average between the estimations based on Eqs. (4) and (5). Again, a smooth variation with Nb content is obtained and a single scatter band accounts for the data on Ω^q and Ω^a. It has long been believed [3] that the isothermal Ω^a phase is characterized by a $c_\Omega/a_\Omega \cong 0.622$, whereas the athermal Ω^q phase shows a lower c_Ω/a_Ω, approaching that of the β phase, viz., $c_\Omega/a_\Omega \cong 0.6124$. The present analysis suggests, however, that the main cause of the observed difference in the c_Ω/a_Ω ratio is the fact that composition changes occur on aging, which significantly decrease the Nb content in Ω^a.

7. Summary and remarks

The structural and bonding properties of the Ω phase have been the subject of continuous experimental and theoretical interest. Much of the previously published work has been devoted to the $\beta \rightarrow \Omega$ transformation induced by quenching, whereas the physical properties of the Ω phase formed upon aging has not been known in detail. The main goals of the present study have been to add to the understanding of the structural properties and high-temperature reactions of the phases occurring metastably in quenched Zr–Nb alloys, and to develop a picture of these properties able to account consistently for the information about the as-quenched state and the aging experiments. In order to establish the structural relations between these structures, a series of neutron thermodiffractometric experiments have been performed in which the evolution of the system toward equilibrium has been monitored through LP measurements. In addition, a new method of analysis has been developed, which involves a modeling of the LP vs. composition relations in the β and Ω phases as functions of temperature. The method leads to a consistent description of the LPs for the Ω^q and Ω^a phases. In addition, various estimates of the Nb content of the Ω^a phase have been obtained, which provide indirect information of both theoretical and practical interest. In particular, when applied to the available LP data for aged alloys, the present method of analysis reveals a significant depletion in the Nb content of the Ω^a phase. According to the present results, the Ω^a phase contains less than 5 at.% Nb.

In conclusion, a unified picture of the structural systematics of the quenched and aged Ω phase has been arrived at in the present work, which relies on a quantitative account of the significant composition changes induced by aging. This of course does not exclude the possibility that other factors might contribute to the observed differences between the quenched and aged Ω phase. The main finding of the present study is that the composition changes occurring upon evolution toward equilibrium probably represent the crucial factor, but not necessarily the unique one.

Acknowledgements

The alloys and samples were prepared by C. Ayala at the Metals Physics Division (Centre Atómico Bariloche, Argentina). Chemical analyses of impurities were performed at CONUAR SA. Some of the samples for microanalysis were mounted by M. Zalazar at Universidad Nacional del Comahue, and the EPMA measurements were performed by G. López at Max-Planck-Institut für Met-allforschung, Stuttgart. We appreciate the support of the Spanish Cooperation Research Group at the Institut Laue-Langevin, which allowed us to use the D1B neutron diffractometer. This work is part of a research project supported by Agencia Nacional de Promoción Científica y Tecnológica (Argentina), under grant No. 03-00000-00688 and by CONICET (Argentina) under grant PIP 02612.

References

[1] R.A. Deegan, J. Phys. C 1 (1968) 763;
N.W. Dalton, R.A. Deegan, J. Phys. C 2 (1969) 2369;
J. Friedel, in: J.M. Ziman (Ed.), The Physics of Metals, Cambridge, UK, 1969;
D.G. Pettifor, J. Phys. C 3 (1970) 367;
J.C. Duthie, D.G. Pettifor, Phys. Rev. Lett. 38 (1977) 564;
D.G. Pettifor, J. Chem. Phys. 69 (1978) 2930;
H.L. Skriver, Phys. Rev. B 31 (1985) 1909.
[2] A.P. Miodownik, in: P.E.A. Turchi, A. Gonis (Eds.), Statics and Dynamics of Alloy Phase Transformations, Plenum, NY, 1994, p. 45.

[3] S.K. Sikka, Y.K. Vohra, R. Chidambaram, Prog. Mater. Sci. 27 (1982) 245.
[4] D. de Fontaine, Metall. Trans. A 19 (1988) 169.
[5] K.-M. Ho, C.-L. Fu, B.N. Harmon, Phys. Rev. B 29 (1984) 1575;
J.A. Moriarty, Phys. Rev B 45 (1992) 2004;
R. Ahuja, J.M. Wills, B. Johansson, O. Eriksson, Phys. Rev. B 48 (1993) 16269;
I. Bakonyi, H. Ebert, A.I. Liechtenstein, Phys. Rev. B 48 (1993) 7841;
D. Nguyen-Mahn, D.G. Pettifor, G. Shao, A.P. Miodownik, A. Pasturel, Philos. Mag. A 74 (1996) 1385.
[6] J.E. Garcés, G.B. Grad, A. Fernández Guillermet, S.J. Sferco, J. Alloys Comp. 287 (1999) 6;
J.E. Garcés, G.B. Grad, A. Fernández Guillermet, S.J. Sferco, J. Alloys Comp. 289 (1999) 1.
[7] G.B. Grad, P. Blaha, J. Luitz, K. Schwarz, A. Fernández Guillermet, S.J. Sferco, Phys. Rev. B 62 (2000) 12743.
[8] H. Xia, G. Parthsarthy, H. Luo, Y.K. Vohra, A.L. Ruoff, Phys. Rev. B 42 (1990) 6736;
J.P. Perdew, K. Burke, M. Ernzerhof, Phys. Rev. Lett. 77 (1996) 3865;
K.D. Joshi, G. Jyoti, S.C. Gupta, S.K. Sikka, Phys. Rev. B. 65 (2002) 52106;
I.O. Bashkin, V.K. Fedotov, M.V. Nefedova, V.G. Tissen, E.G. Ponyatovsky, A. Schiwek, W.B. Holzapfel, Phys. Rev. B 68 (2003) 54401.
[9] A. Fernández Guillermet, in: J. Martínez Mardones, C.H. Wörner, J. Walgraef (Eds.), Materials Instabilities, World Scientific, Singapore, 2000, p. 1;
A. Fernández Guillermet, J. Phase Equilib. 23 (2002) 470.
[10] A. Fernández Guillermet, Z. Metallkd. 82 (1991) 478;
H. Okamoto, J. Phase Equilib. 13 (1992) 577.
[11] G. Aurelio, A. Fernández Guillermet, G.J. Cuello, J. Campo, J. Alloys Comp. 335 (2002) 132.
[12] D.J. Cometto, G.L. Houze Jr., R.F. Hehemann, Trans. Met. Soc. AIME 233 (1965) 30.
[13] M. Suenaga, J.L. O'Brien, V.F. Zackay, K.M. Rails, Trans. Met. Soc. AIME 239 (1967) 992.
[14] N.A. Vanderpuye, A.P. Miodownik, in: R.I. Jaffee, N.E. Promisel (Eds.), The Science Technology and Applications of Titanium, Pergamon, New York, 1970, p. 719.
[15] G. Aurelio, A. Fernández Guillermet, G.J. Cuello, J. Campo, Met. Mater. Trans. 34A (2003) 2771.
[16] G. Aurelio, A. Fernández Guillermet, J. Alloys Comp. 292 (1999) 31;
G. Aurelio, A. Fernández Guillermet, J. Alloys Comp. 298 (2000) 30;
G. Aurelio, A. Fernández Guillermet, Z. Metallkd. 91 (2000) 35.
[17] G.J. Cuello, A. Fernández Guillermet, G.B. Grad, R.E. Mayer, J.R. Granada, J. Nucl. Mater. 218 (1995) 236.
[18] G.B. Grad, A. Fernández Guillermet, J.J. Pieres, G.J. Cuello, Z. Metallkd. 87 (1996) 721.
[19] B. Olinger, J.C. Jamieson, High Temp. High Press. 5 (1973) 123.
[20] E.N. Kaufmann, D.B. McWhan, Phys. Rev. B 8 (1973) 1390.
[21] T. Butz, G.M. Kalvius, H. Göbel, W.B. Holzapfel, Hyperfine Interact. 1 (1975) 1.
[22] G.M. Benites, A. Fernández Guillermet, J. Alloys Comp. 302 (2000) 192.
[23] J.P. Guérillon, Metaux, Corrosion, Industrie 557 (1972) 21.
[24] L. Pauling, J. Am. Chem. Soc. 69 (1947) 542.
[25] J.C. Jamieson, Science 140 (1963) 72.
[26] G.J. Cuello, G. Aurelio, A. Fernández Guillermet, G.M. Benites, J. Campo, Scr. Mater. 44 (2001) 2821.
[27] G.B. Grad, A. Fernández Guillermet, J.R. Granada, Z. Metallkd. 87 (1996) 726.
[28] G.M. Benites, G. Aurelio, A. Fernández Guillermet, G.J. Cuello, F.J. Bermejo, J. Alloys Comp. 284 (1999) 251.
[29] G. Aurelio, PhD thesis, Institute Balseiro – Universidad Nacional de Cuyo, Bariloche, Argentina, 2003.
[30] J. Rodríguez-Carvajal, FULLPROF: A Program for Rietveld Refinement and Pattern Matching Analysis, Abstracts of the Satellite Meeting on Powder Diffraction of the XV Congress of the IUCr, 127, Toulouse, France, 1990.
[31] G.M. Benites, A. Fernández Guillermet, G.J. Cuello, J. Campo, J. Alloys Comp. 299 (2000) 183.
[32] G.B. Grad, J.J. Pieres, A. Fernández Guillermet, G.J. Cuello, J.R. Granada, R.E. Mayer, Physica B 213 (1995) 433.
[33] D.J. Cometto, PhD thesis, Case Institute of Technology, 1962.
[34] M. Chaturvedi, K. Tangri, Trans. Met. Soc. AIME 245 (1969) 259.
[35] M. Chatuverdi, R.N. Singh, J. Less-Comm. Metals 18 (1969) 71.
[36] G.B. Grad, J.J. Pieres, A. Fernández Guillermet, G.J. Cuello, R.E. Mayer, J.R. Granada, Z. Metallkd. 86 (1995) 395.
[37] G. Aurelio, A. Fernández Guillermet, G.J. Cuello, P.B. Bozzano, Mater. Sci. Forum 480–481 (2005) 565.
[38] G. Aurelio, P.B. Bozzano, A. Fernández Guillermet, Arch. Metall. Mater. 49 (2004) 453.
[39] R.F. Hehemann, S.T. Zegler, Trans. Met. Soc. AIME 236 (1966) 1594.
[40] G. Aurelio, A. Fernández Guillermet, G.J. Cuello, J. Campo, Metall. Trans. A 32 (2001) 1903.